Desalination and Water Treatment
www.deswater.com

doi: 10.5004/dwt.2017.21070

85 (2017) 175–183
August

Kinetics, isotherms, and thermodynamic modeling of liquid-phase adsorption of Rhodamine B dye onto Fe/ZnO-shrimp shell nanocomposite

Zohreh Saadati*, Masomeh Gilani

Department of Chemistry, Islamic Azad University, Omidiyeh Branch, Omidiyeh, Iran, Tel. +98 9166145685; Fax: +98 6152622533; emails: saadati.z@iauo.ac.ir, zohrehsaadati@gmail.com (Z. Saadati), Tel. +98 9167867175; email: masome.gilani@yahoo.com (M. Gilani)

Received 10 January 2017; Accepted 24 June 2017

ABSTRACT

A cost-efficient nanocomposite was synthesized by sol–gel production of Fe^{3+}-doped ZnO nanoparticles (Fe–ZnO) on a base of shrimp shell. Samples were characterized using X-ray power diffraction, Fourier transform infrared spectrometry, and scanning electron microscopy through energy-dispersive X-ray analysis. Experimental studies on the removal of Rhodamine B (RB) from an aqueous solution in batches revealed that the adsorption equilibrium was best represented by the Langmuir isotherm, with a maximum monolayer capacity of 83.81 mg g^{-1} for RB. Kinetic data were well described by a pseudo-second-order kinetic model. Different thermodynamic parameters, that is, changes in standard free energy, enthalpy, and entropy, were also evaluated. It was found that dye adsorption into the nanocomposite was a spontaneous, exothermic, and physical reaction.

Keywords: Fe^{3+}-doped ZnO nanoparticle; Shrimp shell; Adsorption isotherms; Adsorption kinetics

1. Introduction

The recent rate of population growth has led to rapid industrialization that has accelerated environmental pollution. Textile industries discharge a large volume of dyes into water sources. Some of these dyes are known to be mutagenic and carcinogenic to the human body [1]. Textile-dyeing effluents are characterized by three parameters: (1) pH fluctuation with suspended particles, (2) high oxygen demand, and (3) non-biodegradability and stability to many oxidizing agents [2,3]. The cation dye Rhodamine B (RB) is one of the most commonly used xanthene dyes in the textile industry, and has been found to be potentially toxic and carcinogenic. As a result, it has been banned from use in foods and cosmetics [4,5]. The dye wastewater, if not disposed properly, can lead to severe ecological destruction, especially if discharged directly into the river, as is still common practice in some low-income countries [6–8].

There has been a strong interest in inorganic–organic composites at nanoscale dimensions because of various problems resulting from different types of dye-removal agents. In these materials, inorganic and organic components are blended or hybridized in virtually any combination at the nanometer scale to form hybrid/nanocomposite materials [9–13]. In addition, metal oxide nanoparticles have wide and important applications for manufacturing commercial and personal products. Different inorganic metal-oxide nanoparticles are being synthesized; however, ZnO nanomaterials have attracted particular interest due to their unique and fascinating optical, electrical, mechanical, and piezoelectric properties. ZnO has many applications in fundamental research, along with the potential for use in hydrogen storage [14], field emitters [15], gas sensors [16], ultraviolet lasers [17], solar cells [18], piezoelectric devices [19], and photocatalysts [20].

Coagulation, chemical oxidation, adsorption, microbial degradation, ion-exchange [21,22], and photocatalysis are the most common dye-removal techniques [23,24]. Of these techniques, adsorption is more promising than other available water treatment techniques, due to its flexibility, convenience, low levels of pollutants, and cost-effectiveness [25–29]. Therefore, several low-cost adsorbents such as hen

* Corresponding author.

feather [30], bottom ash [31], cannabinus fiber [32], egg shells [33], and alginate [34,35] have been used for dye treatment. However, the adsorption capacity of absorbents varies with the type of dyes. Carbonaceous materials such as carbon nanotubes [36] and activated carbon may be effective for multiple types of dyes; however, treatment may be expensive.

Metal-ion doping is the most effective approach to improve the ability of ZnO applications to induce structural modifications [37]. Currently, M-doped ZnO nanoparticles are developed to use a metallic or non-metallic M fragment for photodegradation of organic dyes [38–42]. Recently, nanocomposites based on TiO_2, BiOCl, Fe_2O_3, CuS, and ZnO have been used to remove dyes and metal from wastewater [43–46]. Nanocomposites based on biomaterial have drawn considerable attention because of their low cost, easy processability, high-volume application, renewable nature, and possibility of recycling [47].

In this project, shrimp shells were used as the base for a nanocomposite. One of the major components of shrimp shell is chitin, which constitutes 16%–20% of raw shrimp shell [48]. Chitin, the second most abundant polysaccharide in nature after cellulose, has a high sorption capacity that is associated with the presence of –OH and *N*-acetyl groups; it has been widely studied for the removal of various pollutants [49]. The present study aims to characterize the Fe/ZnO-shrimp shell nanocomposite using X-ray diffraction (XRD), Fourier transform infrared spectrometry (FTIR), and scanning electron microscopy (SEM) through energy-dispersive X-ray analysis (EDX) to investigate dye removal at different adsorbent dosages, initial pH, dye initial concentration, and contact time. Meanwhile, adsorption isotherm, kinetics, thermodynamics, and regeneration experiments are also evaluated.

2. Experimental setup

2.1. Materials

RB ($C_{28}H_{31}ClN_2O_3$, molecular weight 479.01 g mol^{-1}), dye content 95%, was procured from M/s. Sigma-Aldrich (Malaysia) and used without further purification. All concentrations of RB solutions were prepared from its 1,000 mg L^{-1} stock solution. Zinc acetate dehydrate, absolute ethanol, iron(III) nitrate ($Fe(NO_3)_3$–$9H_2O$), and oxalic acid were purchased from M/s. Merck Chemical Company (Malaysia). All chemicals were used without further purification.

2.2. Preparation of shrimp shells

First, shrimp shells were obtained from a local market, and the exoskeletons were manually removed, washed, dried, and ground to pass through a 60-mesh sieve. Subsequently, the ground shrimp shells were stirred using a magnetic stirrer; distilled water and HCl were added to produce completely clean and white exoskeletons, which were passed through a filter, and then placed in an oven for 24 h at 100°C to be completely dried.

2.3. Preparation of Fe/ZnO-shrimp shell nanocomposite

Fe^{3+}-doped ZnO nanoparticles (Fe–ZnO) were synthesized by a sol–gel method using zinc acetate, oxalic acid, and iron nitrate as initial materials. A solution of zinc acetate was made by dissolving zinc acetate in 100 mL of alcohol, then heating the mixture in a water bath at 65°C ± 5°C under reflux for 30 min (solution A). Additionally, the oxalic acid solution was prepared by dissolving the oxalic acid in 50 mL of alcohol while stirring with a magnetic stirrer for 30 min (solution B). The required amount of iron nitrate (iron content was 10.0%, which was determined as nFe/(nFe + nZn) × 100 or ZnO–10Fe) was dissolved in 20 mL of ethanol under ultrasonication and added to solution A while continuously stirring. Solution B was slowly added by drops to solution A under vigorous magnetic stirring until a gel was formed [50,51]. The shrimp shells (1 g) were added to the solution. The gel was continuously stirred for another 60 min. The resulting gel was dried in an oven at 80°C for 5 h, then calcined at 200°C for 2 h.

2.4. Characterization of shrimp shell and Fe/ZnO-shrimp shell nanocomposite

FTIR spectra were recorded as pressed KBr discs using a PerkinElmer RXI FTIR instrument. The phase composition and the crystallite size of shrimp shell and nanocomposite samples were determined using an XRD model D8 Advance Bruker AXS X-ray with Cu Kα radiation (1.5406 Å) in the scan range of 2θ from 20° to 80°. The morphology of the particles was studied using a scanning electron microscope, TESCAN Vega Model under high resolution mode, along with the EDX system.

2.5. Batch adsorption studies

Adsorption experiments were carried out by adding a fixed amount of nanocomposite to a series of Erlenmeyer flasks filled with 25 mL of diluted solutions. The Erlenmeyer flasks were shaken at room temperature for 3 h at 300 rpm. After equilibration, 10 mL of the suspension was centrifuged in a tube stoppered at 3,000 rpm for 10 min, and 4 mL of the dye solution was taken from the tube using a filtered syringe for measurement. The absorption of dye concentrations was measured using a PerkinElmer model UV/Vis spectrophotometer for maximum absorbance wavelength values (λ_{max} = 554 nm) for RB dye. To determine the optimum conditions, several parameters such as contact time, pH, initial dye concentration, adsorbent dose, and temperature were studied for RB dye. Using optimum conditions, dye-removal capacity, equilibrium values, and kinetic studies were performed for RB dye.

3. Results and discussion

3.1. FTIR analysis

FTIR spectroscopy was used in the characterization of the shrimp shells, nanocomposite (before and after adsorption), and RB dye. The FTIR spectra of shrimp shells indicate a broad band at 3,447.80 cm^{-1} attributed to –NH_2 and –OH groups' stretching vibrations of chitin and chitosan molecules in shrimp. The peaks at 1,657 and 1,557 cm^{-1} are attributed to a C=O carbonyl group connected to amide I and amides groups, indicating the presence of an acetyl amino group of chitin in shrimp. The peak at 2,932 cm^{-1} is related to –CH

stretching vibrations, and peaks at 1,157, 1,073, and 1,026 cm^{-1} can be attributed to C–O–C asymmetrical stretching.

The FTIR spectrum of RB indicates a broad band at 1,697 cm^{-1}, which can be attributed to the presence of a carbonyl group C=O, the peaks at 1,400–1,600 cm^{-1} can be attributed to aromatic rings, a broad band at 2,975 cm^{-1} is related to CH alkane groups, and peaks at 1,000–1,350 cm^{-1} are attributed to the presence of a C–N bond.

FTIR spectra were recorded for the nanocomposite before adsorption. Given that the base of the nanocomposite is shrimp shell and a bioadsorbent, the high temperature required for calcination of Fe–ZnO had to be adjusted. Therefore, the calcination was performed at multiple temperatures, and the FTIR spectrum was studied. It was calcined at 150°C and 200°C for 2 h and at 400°C for 2 h. The optimum temperature was 200°C. Significant peaks for shrimp showed no change. The broad band at 1,628 cm^{-1} was attributed to the carbonyl group. The peak at 1,465 cm^{-1} was related to Si–O in the shrimp shell, while the peaks at 536 cm^{-1} indicated the stretching frequency of Zn–O and 490 cm^{-1} related to the Fe group.

FTIR spectra were recorded for the nanocomposite after adsorption. The broad band at 3,399 cm^{-1} can be attributed to $–NH_2$ and –OH groups' stretching vibration of chitin and chitosan molecules in the shrimp shell, and the peaks at 1,663 cm^{-1} are related to the C=O carbonyl group connected to the amides I and amides groups, indicating the presence of an acetyl amino group of chitin in the shrimp shell. The peaks at 2,931–1,600 cm^{-1} is attributed to –CH stretching vibration, while the peak at 747 cm^{-1} is related to Al–O in the shrimp shell. The peaks at 1,000–1,350 cm^{-1} are attributed to the N–C bond in the RB dye, and the transmission peaks at 534 and 495 cm^{-1} are, respectively, related to Zn–O and Fe; the peak intensity of both peaks decreased after adsorption.

Fig. 1 shows the XRD pattern of the shrimp shell and nanocomposite Fe/ZnO-shrimp shell. Relatively broad diffraction peaks for shrimp shells of 2θ = 10° and 2θ = 20° are related to the semicrystalline structures of chitosan [52].

The XRD spectrum of the nanocomposite Fe/ZnO-shrimp shell shows that Fe^{3+} is well doped by calcining at 200°C for 2 h. This pattern also showed the hexagonal structure of ZnO nanoparticles (2θ = 34.07°, 35.69°, 37.83°, 47.91°, and 57.006°) [53]. A diffraction band of Fe-doped ZnO sample does not show the existence of pure iron, but does indicate the existence of Fe_2O_3. This can probably be attributed to good dispersion of Fe^{3+} inside the ZnO network structure. The scan value of 2θ = 23° is related to Fe–O that has been shifted.

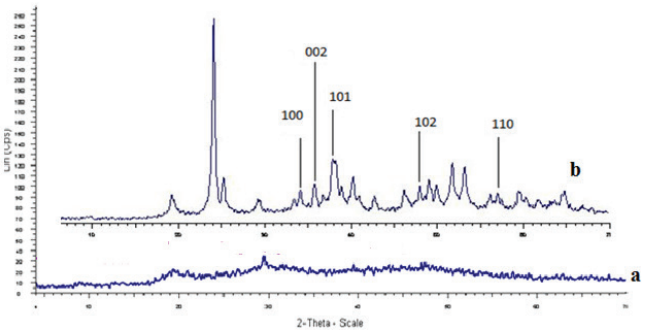

Fig. 1. XRD patterns of shrimp shell (a), and nanocomposite Fe/ZnO-shrimp shell (b).

3.2. Morphology of shrimp shells and nanocomposite

The morphology of shrimp shells and nanocomposite was investigated using SEM/EDX (Figs. 2 and 3). Results indicated that shrimp shell contains inorganic compounds consisting of Al, Si, Ca, and P in addition to the organic compounds chitosan and chitin.

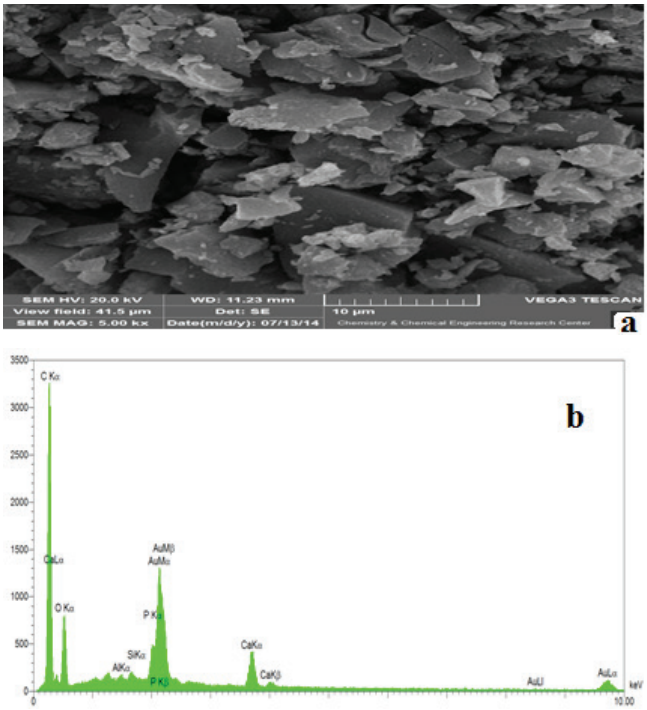

Fig. 2. SEM micrograph (a) and EDX spectrum (b) of shrimp shell.

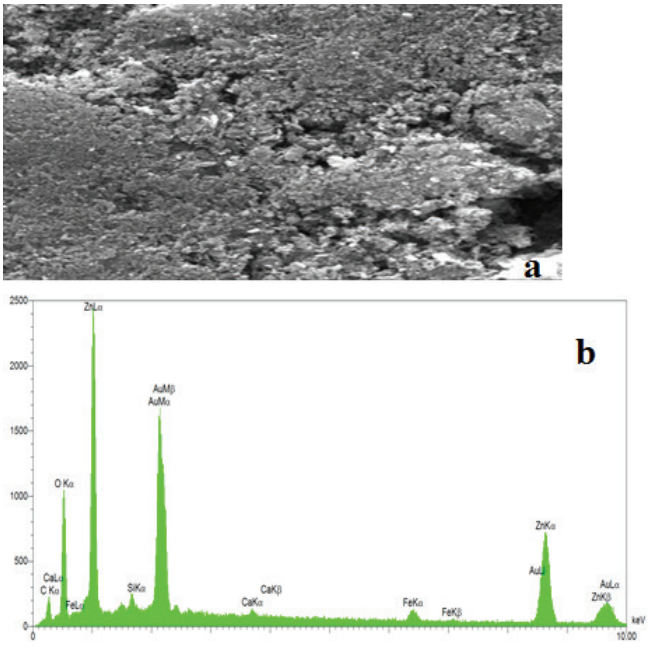

Fig. 3. SEM micrograph (a) and EDX spectrum (b) of nanocomposite.

The analysis of SEM/EDX data showed that the major elements of the nanocomposite were O and Zn. The lower amount of Fe compared with Zn indicates effective Fe coating. According to the results, phosphorus in the shrimp shells was removed after calcination. However, chlorine remained in the nanocomposite by adding hydrochloric acid. The SEM/EDX was carried out on the ZnO–10.0Fe samples to determine the average (bulk) iron content. The spectra clearly indicated the presence of iron ($\frac{n_{Fe}}{n_{Zn}+n\text{Fe}}$); the atomic ratio was found to be 10.2%. This is in good agreement with the nominal iron concentrations in the sample [54].

3.3. Effect of different parameters

3.3.1. Effect of pH

Dye molecules mainly interact with the adsorbent particles by electrostatic interaction, hydrophobic–hydrophobic interaction, and hydrogen bonding. Due to the adsorption system's direct influence on electrostatic interaction, the effect of pH is important. The effect of pH of the solution on the adsorption efficiency of RB is given in Fig. 4. RB removal was the highest at an initial pH value of 4. As the pH value increased, the amount removed began to decrease. At solution pH < 4.0, the RB molecules existed in cationic and monomeric forms, forming dimer at solution pH values > 4.0, due to RB molecules in zwitterionic form. More RB was removed for pH > 4.0 than for the rest of the pH range, even though RB molecules were positively charged at pH = 4. This indicates that electronic interaction might not be the main force in the interaction between adsorbate and adsorbent. Furthermore, smaller amounts of monomeric RB may diffuse into the micropores of the adsorbent particle more easily than the dimer form [55,56].

3.3.2. Effect of adsorbent dose

To study variation in adsorption on the basis of the amount of the adsorbent materials, various amounts from 0.04 to 0.25 g of adsorbent were chosen. Increasing the amount of adsorbent dosage from 0.04 to 0.15 g led to a gradual rise in the amount of RB dye removed until a dosage of 0.15 g, after which an insignificant increase was observed (Fig. 5).

This trend is due to the increase in active sites for the adsorption of RB by increasing the adsorbent dosage. Meanwhile, a high adsorbent dose led to little improvement in dye adsorption. This could be due to a higher collision rate between the adsorbent particles, resulting in fewer vacant sites per unit mass of adsorbent available for adsorption, as such collisions can cause active sites to overlap or aggregate [57]. Therefore, the amount of 0.15 g was chosen as the optimal dose of adsorbent.

3.3.3. Effect of contact time

All data from the contact time experiment was obtained at different contact times with a fixed dose of nanocomposite (0.15 g), initial dye concentration 6 mg L^{-1}, solution pH of 4, and temperature of 25°C (Fig. 6). The results showed that the removal efficiency of RB rises rapidly with time until it reaches equilibrium, after which it remains constant.

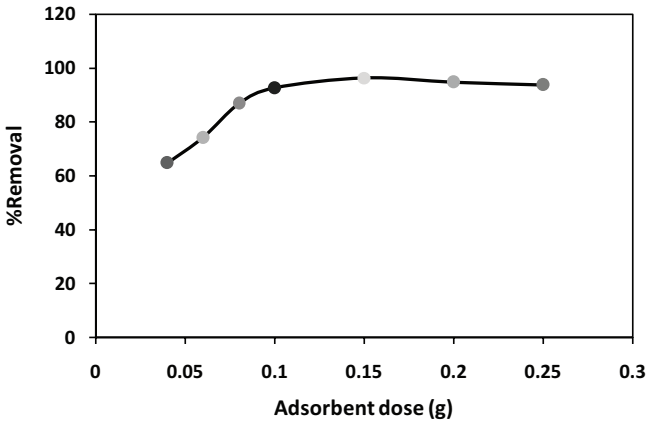

Fig. 5. The effect of adsorbent dose on the removal of RB by the nanocomposite (contact time 3 h, pH 4, initial concentration of dye 6 mg L^{-1}, and temperature of 25°C).

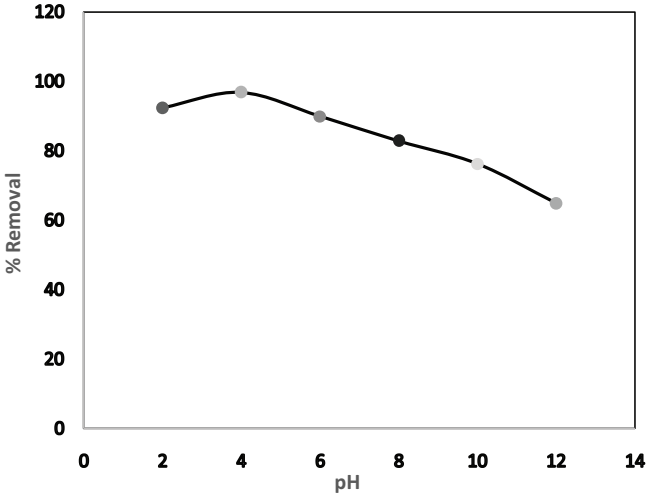

Fig. 4. The effect of pH on the removal of RB by the nanocomposite (contact time 3 h, adsorbent dose 0.1 g, concentration of dye 6 mg L^{-1}, and temperature 25°C).

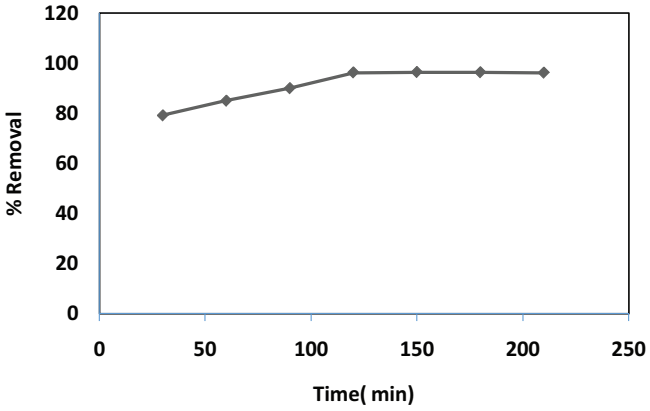

Fig. 6. The effect of contact time on the removal of RB by the nanocomposite (adsorbent dose 0.15 g, pH 4, initial concentration of dye 6 mg L^{-1}, and temperature 25°C).

In addition, the contact time to reach equilibrium is equal to 120 min at 96.31% of dye-removal percentage. This result was expected due to the availability of a large number of surface sites for adsorption at the initial stages. After a lapse of time, the remaining surface sites are difficult to fill because of repulsive forces between the solute molecules of the solid and bulk phases [58].

3.3.4. Effect of dye concentration

The influence of dye concentration on the adsorption capacity of nanocomposite is indicated in Fig. 7. The increase of dye concentration resulted in a lower percentage of RB removed. The dye/sorbent ratio increases as sorption sites are saturated, leading to decreasing sorption efficiency [59].

3.3.5. Effect of temperature

Adsorption experiments were performed at different temperatures with a constant RB concentration of 6 mg L^{-1}, adsorbent dosage of 0.15 g, and pH 4. The percentage of RB removed decreases with increasing temperature, showing that sorption is an exothermic process. The thermodynamic parameters in the adsorption process, $\Delta H°$, $\Delta S°$, and $\Delta G°$, were calculated through the following equations:

$$\Delta G° = -RT \ln K \quad (1)$$

$$\ln K = \frac{\Delta S^{\circ}}{R} - \frac{\Delta H^{\circ}}{R} \quad (2)$$

$$\Delta G° = \Delta H° - T\Delta S° \quad (3)$$

where K, known as the distribution coefficient of the adsorbate, is equal to (q_e/C_e). R is the gas constant (8.314 J mol K^{-1}), and T is the temperature in kelvin. As shown in Fig. 8, the plot of ln$K$ vs. 1/T is linear with the slope and the intercept, giving the values of $\Delta H°$ and $\Delta S°$. These values can be used to calculate $\Delta G°$. All these relations are valid when the enthalpy change remains constant over the temperature range. These thermodynamic parameters are shown in Table 1. Generally, the exchange of free energy for physical adsorption is smaller than that for chemical adsorption. The positive value of $\Delta H°$ indicates that the adsorption is an endothermic process, while a positive $\Delta S°$ value reflects the increasing randomness at the solid/solution interface during adsorption. Adsorption of solute from the solution on a solid surface is a complex phenomenon, and the entropy within the system is determined by degrees of freedom of the adsorbate (solute) and solvent molecules. The positive value of entropy could be due to the affinity of the nanocomposite for RB and the desorption of water molecules from the surface of the adsorbents [60–62]. The changes in free energy for physical and chemical reactions are between –20 and 0 kJ mol^{-1} and between –80 and –400 kJ mol^{-1}, respectively [63].

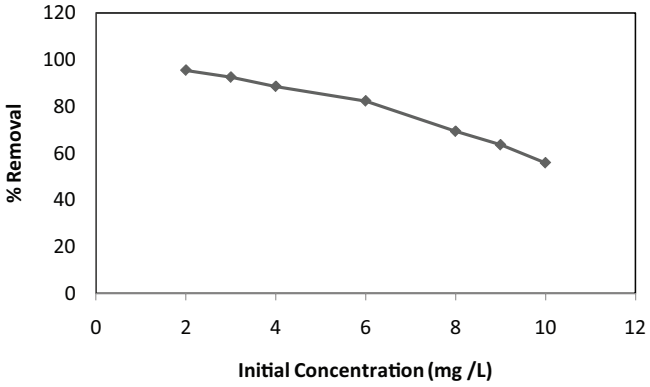

Fig. 7. The effect of dye concentration on the removal of RB by the nanocomposite (contact time 3 h, adsorbent dose 0.15 g, pH 4, and temperature 25°C).

3.4. Adsorption isotherms

The purpose of the adsorption isotherms is to relate the adsorbate concentration in the bulk and the adsorbed amount at the interface [64]. Adsorption isotherms are the most important information for analyzing and designing an adsorption process [65,66]. To describe the isotherms (Fig. 9), initially Langmuir and Freundlich models [67,68] were used (Eqs. (4) and (5)):

$$q_e = \frac{q_m K_L C_e}{1 + K_L C_e} \quad (4)$$

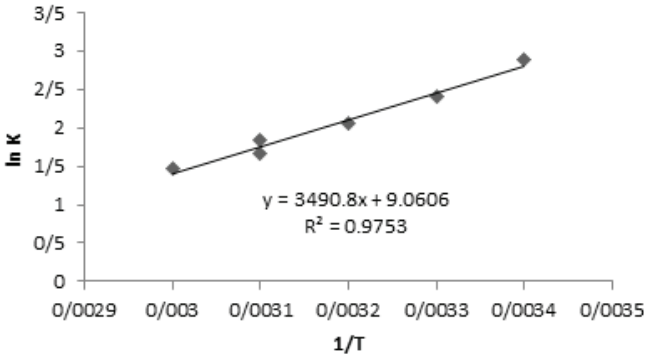

Fig. 8. Plot of ln$K$ vs. 1/T for the estimation of thermodynamic parameters.

Table 1
Thermodynamic parameters for adsorption of RB on nanocomposite at different temperatures

Temperature (K)	$\Delta G°$ (kJ mol^{-1})	$\Delta H°$ (kJ mol^{-1})	$\Delta S°$ (kJ mol^{-1} K^{-1})
298	–71.60	–29.02	0.142
303	–60.45		
308	–52.49		
313	–47.62		
318	–43.88		
323	–39.74		

$$q_e = K_F C_e^{\frac{1}{n_F}} \quad (5)$$

where q_e (mg g^{-1}) is the adsorbed amount of the dye; C_e (mg L^{-1}) is the equilibrium concentration of the dye in solution, q_m (mg g^{-1}) is the maximum adsorption capacity, and K_L (L mg^{-1}) is the energy of adsorption. K_F is adsorption capacity at unit concentration, and $1/n$ is adsorption intensity. Correlation coefficients and other parameters are summarized in Table 2. Generally, for the evaluation of best fit, values of correlation coefficients (R^2) of linear plots of different models were considered [69]. Values of R^2 of a linear plot of the Langmuir model were found to fit better than those of the Freundlich model.

The maximum adsorption capacity (q_m) of the nanocomposite was found to be 83.81 mg g^{-1} for RB. The maximum monolayer adsorption capacities of RB onto various adsorbents are compared in Table 2. It is worth noting that the nanocomposite prepared for this work demonstrates a relatively large adsorption capacity, compared with the data obtained from the literature in Table 3.

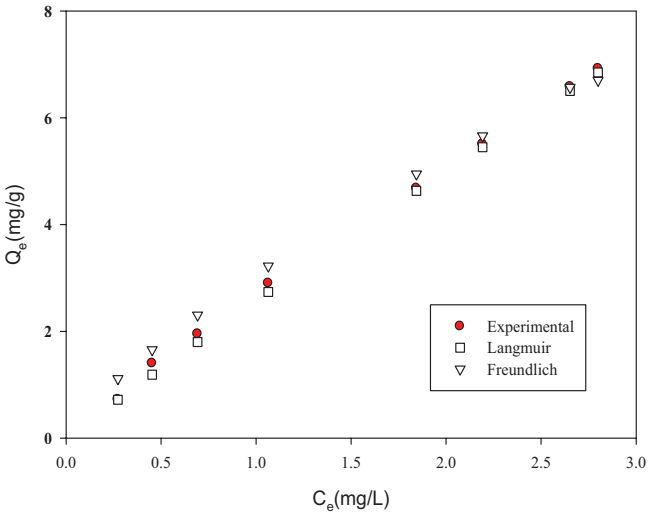

Fig. 9. Adsorption isotherms of RB adsorption on nanocomposite.

Table 2
Langmuir and Freundlich isotherm model constants and correlation coefficients for adsorption of RB adsorption on nanocomposite

Isotherm	Parameters
Langmuir	
q_m (mg g^{-1})	83.81
K_L (L mg^{-1})	0.032
R^2	0.998
Freundlich	
K_F (mg g^{-1})	3.07
n	1.28
R^2	0.976

The important characteristic of the Langmuir isotherm can be expressed by means of the dimensionless constant separation factor, calculated using the following equation:

$$R_L = \frac{1}{1 + K_L C_0} \quad (6)$$

The value of R_L indicates the type of adsorption to be unfavorable ($R_L > 1$), linear ($R_L = 1$), favorable ($0 < R_L < 1$), or irreversible ($R_L = 0$) [76]. Values of R_L were found to be favorable, and decreased from 0.45 to 0.15 for C_o 2–10 mg L^{-1}.

3.5. Adsorption kinetics

The sorption dynamics of RB with the nanocomposite were evaluated by adding 0.15 g of Fe/ZnO-shrimp nanocomposite to 100 mL of a mixed solution containing 2 mg L^{-1} RB (pH 4.0) at room temperature. The concentration of RB in solution was measured after the nanocomposite adsorption was taken for 30, 60, 90, 120, 150, 180, and 210 min.

A linear form of pseudo-first-order model was described by Lagergren [77] in the form:

$$\log\left(q_e - q_t\right) = \log q_e - \frac{K_1}{2.303} \quad (7)$$

A linear plot of $\log(q_e - q_t)$ against time allows one to obtain the rate constant (Fig. 10). If the plot is linear with a

Table 3
Comparison of the maximum monolayer adsorption capacities of RB on various adsorbents

References	q_m (mg g^{-1})	Adsorbent
[70]	71	Coconut (*Cocos nucifera*)
[71]	13.76	Rice husk ash
[72]	41	Cocoa (*Theobroma cacao*) shell
[73]	67	Perlite
[74]	111	NiO nanoparticles
[75]	128.2	ZnO-activated carbon
This work	83.81	

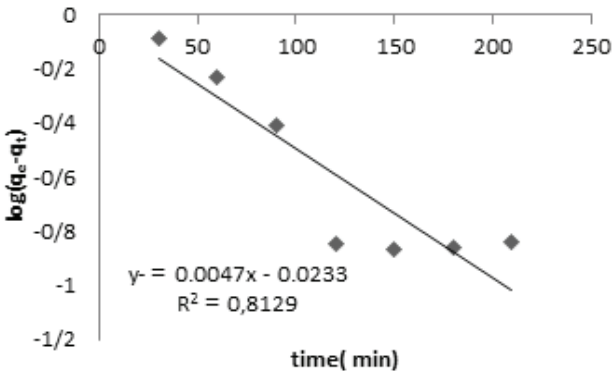

Fig. 10. Pseudo-first-order sorption kinetics for RB sorption onto nanocomposite.

Table 4
Comparison of the pseudo-first-order, pseudo-second-order adsorption rate constants, and calculated and experimental q_e values obtained at different initial RB concentrations

Kinetic model	Parameters
Pseudo-first-order	
$q_{e,cal}$ (mg g^{-1})	0.9
k_1 (min^{-1})	0.0069
R^2	0.817
Pseudo-second-order	
k_2 (g mg^{-1} min^{-1})	0.018
$q_{e,cal}$ (mg g^{-1})	2.02
h (mg min^{-1} g^{-1})	0.710
R^2	0.994
$q_{e,exp}$ (mg g^{-1})	1.99

good correlation coefficient, it is indicated that Lagergren's equation is appropriate to RB sorption on nanocomposite. Thus, the adsorption process is a pseudo-first-order process [77,78]. The Lagergren's first-order rate constant (k_1) and q_e determined from the model are presented in Table 4 along with the corresponding correlation coefficients. It was observed that the pseudo-first-order model did not fit well. It was found that the calculated q_e value did not agree with the experimental q_e value. This suggests that the adsorption of methylene blue does not follow first-order kinetics.

The pseudo-second-order kinetics may be expressed in a linear form as [79,80]:

$$\frac{t}{q_t} = \frac{1}{k_2 q_e^2} + \frac{t}{q_e} \tag{8}$$

where the equilibrium adsorption capacity (q_e) and the second-order constants k_2 (g mg^{-1} min^{-1}) can be determined experimentally from the slope and intercept of plot t/q_t vs. t (Fig. 11). Values for k_2 and q_e determined from the model are presented in Table 4 along with the corresponding correlation coefficients.

The values of the calculated and experimental q_e are represented in Table 4; there is an agreement between q_e experimental and q_e calculated values for the pseudo-second-order model. Hence, the pseudo-second-order model better represents the adsorption kinetics.

3.6. Reusability of adsorbent

The trivial characteristic feature of an adsorbent in a practical application is its lifetime, because longer periods of time lead to a significant reduction in the cost of the treatment [81]. Hence, the reusability and regeneration of nanocomposite was evaluated for four cycles of adsorption and desorption of RB molecules. The adsorption processes were carried out at pH 4.0, RB concentration of 2 mg L^{-1}, nanocomposite dosage of 1.5 g L^{-1}, temperature of 298 K, and contact time of 120 min, which were the values determined to be the optimum conditions for dye removal.

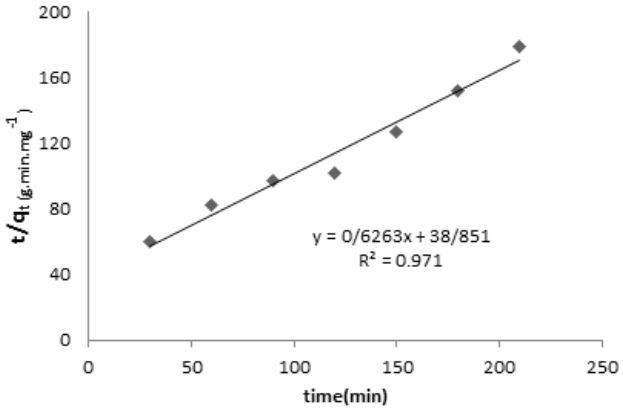

Fig. 11. Pseudo-second-order sorption kinetics for RB sorption onto nanocomposite.

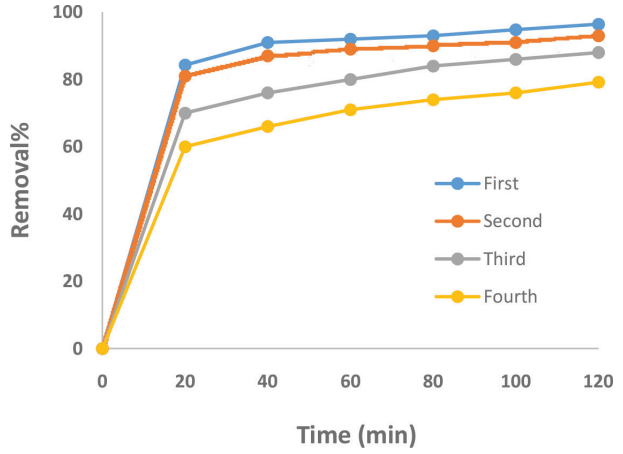

Fig. 12. Regeneration cycles for adsorption of RB by Fe/ZnO-shrimp nanocomposite.

As shown in Fig. 12, the adsorption activity of Fe/ZnO-shrimp nanocomposite decreased slightly after the fourth recycling, and the removal rate for RB was 79.21% in 120 min. Compared with the first recycling (96.44%), the removal rate of fourth only decreased 17.23% within 120 min, indicating that the Fe/ZnO-shrimp nanocomposite is a highly efficient, stable, and reusable sorbent. In this study, the sample was desorbed using absolute ethyl alcohol; thus the Fe/ZnO-shrimp nanocomposite can be regenerated simply through filtration and drying.

4. Conclusion

The present investigation showed that Fe/ZnO-shrimp shell nanocomposite can be effectively used as an adsorbent. To verify the performance of the prepared nanocomposite as an adsorbent, it was employed to remove textile dye, RB, from wastewater. Equilibrium adsorption data were fitted using Langmuir and Freundlich isotherms. The results revealed that the Langmuir isotherm model, with a maximum monolayer adsorption capacity of 83.81 mg g^{-1}, fit the data. Kinetic studies suggested that the process followed the pseudo-second-order kinetic model. The high performance

of the nanocomposite compared with other adsorbents reported in the literature may be due to its porous structure.

Acknowledgment

Authors are grateful to the Research Council at the Islamic Azad University of Omidiyeh for their support.

References

[1] G. Crini, Non-conventional low-cost adsorbents for dye removal: a review, Bioresour. Technol., 97 (2006) 1061–1085.
[2] R. Sivaraj, C. Namasivayam, K. Kadirvelu, Orange peel as an adsorbent in the removal of acid violet 17 (acid dye) from aqueous solutions, Waste Manage., 21 (2001) 105–110.
[3] A.S. Özcan, B. Erdem, A. Özcan, Adsorption of Acid Blue 193 from aqueous solutions onto BTMA-bentonite, Colloids Surf., A, 266 (2005) 73–81.
[4] J.-F. Guo, B. Ma, A. Yin, K. Fan, W.-L. Dai, Photodegradation of rhodamine B and 4-chlorophenol using plasmonic photocatalyst of Ag–AgI/Fe_3O_4@SiO_2 magnetic nanoparticle under visible light irradiation, Appl. Catal., B, 101 (2011) 580–586.
[5] L. Peng, P. Qin, M. Lei, Q. Zeng, H. Song, J. Yang, J. Shao, B. Liao, J. Gu, Modifying Fe_3O_4 nanoparticles with humic acid for removal of Rhodamine B in water, J. Hazard. Mater., 209–210 (2012) 193–198.
[6] T.F. Ahmed, M. Sushil, M. Krishna, Impact of dye industrial effluent on physicochemical characteristics of Kshipra River, Ujjain City, India, Int. Res. J. Environ. Sci., 1 (2012) 41–45.
[7] J. Awomeso, A. Taiwo, A. Gbadebo, J. Adenowo, Studies on the pollution of waterbody by textile industry effluents in Lagos, Nigeria, J. Appl. Sci. Environ., 5 (2010) 353–359.
[8] A. Mittal, Retrospection of Bhopal gas tragedy, Toxicol. Environ. Chem., 98 (2016) 1079–1083.
[9] C. Sanchez, B. Lebeau, F. Ribot, M. In, Molecular design of sol-gel derived hybrid organic-inorganic nanocomposites, J. Sol-Gel Sci. Technol., 19 (2000) 31–38.
[10] M. Wang, Y. Lian, X. Wang, PPV/PVA/ZnO nanocomposite prepared by complex precursor method and its photovoltaic application, Curr. Appl. Phys., 9 (2009) 189–194.
[11] W. Kangwansupamonkon, W. Jitbunpot, S. Kiatkamjornwong, Photocatalytic efficiency of TiO_2/poly[acrylamide-*co*-(acrylic acid)] composite for textile dye degradation, Polym. Degrad. Stab., 95 (2010) 1894–1902.
[12] S. Qin, L. Wang, X. Zhang, G. Su, Grafting poly(ethylene glycol) monomethacrylate onto Fe_3O_4 nanoparticles to resist nonspecific protein adsorption, Appl. Surf. Sci., 257 (2010) 731–735.
[13] X. Gao, Y. Zhu, X. Zhao, Z. Wang, D. An, Y. Ma, S. Guan, Y. Du, B. Zhou, Synthesis and characterization of polyurethane/SiO_2 nanocomposites, Appl. Surf. Sci., 257 (2011) 4719–4724.
[14] Q. Wan, C. Lin, X. Yu, T. Wang, Room-temperature hydrogen storage characteristics of ZnO nanowires, Appl. Phys. Lett., 84 (2004) 124–126.
[15] S. Jo, J. Lao, Z. Ren, R. Farrer, T. Baldacchini, J. Fourkas, Field-emission studies on thin films of zinc oxide nanowires, Appl. Phys. Lett., 83 (2003) 4821–4823.
[16] O. Lupan, L. Chow, S. Shishiyanu, E. Monaico, T. Shishiyanu, V. Şontea, B.R. Cuenya, A. Naitabdi, S. Park, A. Schulte, Nanostructured zinc oxide films synthesized by successive chemical solution deposition for gas sensor applications, Mater. Res. Bull., 44 (2009) 63–69.
[17] H. Yan, R. He, J. Johnson, M. Law, R.J. Saykally, P. Yang, Dendritic nanowire ultraviolet laser array, J. Am. Chem. Soc., 125 (2003) 4728–4729.
[18] A.B. Martinson, J.W. Elam, J.T. Hupp, M.J. Pellin, ZnO nanotube based dye-sensitized solar cells, Nano Lett., 7 (2007) 2183–2187.
[19] X. Ren, D. Han, D. Chen, F. Tang, Large-scale synthesis of hexagonal cone-shaped ZnO nanoparticles with a simple route and their application to photocatalytic degradation, Mater. Res. Bull., 42 (2007) 807–813.
[20] V.K. Gupta, D. Pathania, S. Agarwal, P. Singh, Adsorptional photocatalytic degradation of methylene blue onto pectin–CuS nanocomposite under solar light, J. Hazard. Mater., 243 (2012) 179–186.
[21] M. Naushad, A. Mittal, M. Rathore, V. Gupta, Ion-exchange kinetic studies for Cd(II), Co(II), Cu(II), and Pb(II) metal ions over a composite cation exchanger, Desal. Wat. Treat., 54 (2015) 2883–2890.
[22] A. Mittal, R. Ahmad, I. Hasan, Iron oxide-impregnated dextrin nanocomposite: synthesis and its application for the biosorption of Cr(VI) ions from aqueous solution, Desal. Wat. Treat., 57 (2016) 15133–15145.
[23] R. Wu, J. Qu, H. He, Y. Yu, Removal of azo-dye acid red B (ARB) by adsorption and catalytic combustion using magnetic $CuFe_2O_4$ powder, Appl. Catal., B, 48 (2004) 49–56.
[24] B.K. Körbahti, K. Artut, C. Geçgel, A. Özer, Electrochemical decolorization of textile dyes and removal of metal ions from textile dye and metal ion binary mixtures, Chem. Eng. J., 173 (2011) 677–688.
[25] M. Peydayesh, A. Rahbar-Kelishami, Adsorption of methylene blue onto *Platanus orientalis* leaf powder: kinetic, equilibrium and thermodynamic studies, J. Ind. Eng. Chem., 21 (2015) 1014–1019.
[26] J. Mittal, V. Thakur, A. Mittal, Batch removal of hazardous azo dye Bismark Brown R using waste material hen feather, Ecol. Eng., 60 (2013) 249–253.
[27] H. Daraei, A. Mittal, M. Noorisepehr, J. Mittal, Separation of chromium from water samples using eggshell powder as a low-cost sorbent: kinetic and thermodynamic studies, Desal. Wat. Treat., 53 (2015) 214–220.
[28] H. Daraei, A. Mittal, J. Mittal, H. Kamali, Optimization of Cr(VI) removal onto biosorbent eggshell membrane: experimental & theoretical approaches, Desal. Wat. Treat., 52 (2014) 1307–1315.
[29] R. Ahmad, I. Hasan, A. Mittal, Adsorption of Cr(VI) and Cd(II) on chitosan grafted polyaniline-OMMT nanocomposite: isotherms, kinetics and thermodynamics studies, Desal. Wat. Treat., 58 (2017) 144–153.
[30] A. Mittal, J. Mittal, Hen Feather: A Remarkable Adsorbent for Dye Removal, S.K. Sharma, Ed., Green Chemistry for Dyes Removal from Wastewater, Scrivener Publishing LLC, Salem, Massachusetts, 2015, pp. 409–457.
[31] A. Mittal, L. Kurup, Column operations for the removal and recovery of a hazardous dye 'acid red—27' from aqueous solutions, using waster materials – bottom ash and de-oiled soya, Ecol. Environ. Conserv., 12 (2006) 181–186.
[32] G. Sharma, M. Naushad, D. Pathania, A. Mittal, G. El-Desoky, Modification of *Hibiscus cannabinus* fiber by graft copolymerization: application for dye removal, Desal. Wat. Treat., 54 (2015) 3114–3121.
[33] A. Mittal, M. Teotia, R. Soni, J. Mittal, Applications of egg shell and egg shell membrane as adsorbents: a review, J. Mol. Liq., 223 (2016) 376–387.
[34] A. Mittal, R. Ahmad, I. Hasan, Biosorption of Pb^{2+}, Ni^{2+} and Cu^{2+} ions from aqueous solutions by L-cystein-modified montmorillonite-immobilized alginate nanocomposite, Desal. Wat. Treat., 57 (2016) 17790–17807.
[35] A. Mittal, R. Ahmad, I. Hasan, Poly(methyl methacrylate)-grafted alginate/Fe_3O_4 nanocomposite: synthesis and its application for the removal of heavy metal ions, Desal. Wat. Treat., 57 (2016) 19820–19833.
[36] A. Mittal, M. Naushad, G. Sharma, Z. ALothman, S. Wabaidur, M. Alam, Fabrication of MWCNTs/ThO_2 nanocomposite and its adsorption behavior for the removal of Pb(II) metal from aqueous medium, Desal. Wat. Treat., 57 (2016) 21863–21869.
[37] S. Kumar, S. Mukherjee, R.K. Singh, S. Chatterjee, A. Ghosh, Structural and optical properties of sol-gel derived nanocrystalline Fe-doped ZnO, J. Appl. Phys., 110 (2011) 103508.
[38] P. Korake, R. Dhabbe, A. Kadam, Y. Gaikwad, K. Garadkar, Highly active lanthanum doped ZnO nanorods for photodegradation of metasystox, J. Photochem. Photobiol., B, 130 (2014) 11–19.

[39] M. Mittal, M. Sharma, O. Pandey, UV–Visible light induced photocatalytic studies of Cu doped ZnO nanoparticles prepared by co-precipitation method, Sol. Energy, 110 (2014) 386–397.
[40] R. Saleh, N.F. Djaja, Transition-metal-doped ZnO nanoparticles: synthesis, characterization and photocatalytic activity under UV light, Spectrochim. Acta, Part A, 130 (2014) 581–590.
[41] H. Yoon, B.N. Joshi, S.-H. Na, J.-Y. Choi, S.S. Yoon, Photodegradation of methylene blue of niobium-doped zinc oxide thin films produced by electrostatic spray deposition, Ceram. Int., 40 (2014) 7567–7571.
[42] M.R.R. Kooh, L.B. Lim, L.H. Lim, J. Bandara, Batch adsorption studies on the removal of malachite green from water by chemically modified *Azolla pinnata*, Desal. Wat. Treat., 57 (2016) 14632–14646.
[43] F. Dong, Y. Sun, M. Fu, Z. Wu, S. Lee, Room temperature synthesis and highly enhanced visible light photocatalytic activity of porous BiOI/BiOCl composites nanoplates microflowers, J. Hazard. Mater., 219–220 (2012) 26–34.
[44] V. Gupta, D. Pathania, S. Agarwal, P. Singh, Preparation of cellulose acetate-zirconium (IV) phosphate nanocomposite with ion exchange capacity and enhanced photocatalytic activity, J. Hazard. Mater., 243 (2012) 179–186.
[45] S.-H. Huang, D.-H. Chen, Rapid removal of heavy metal cations and anions from aqueous solutions by an amino-functionalized magnetic nano-adsorbent, J. Hazard. Mater., 163 (2009) 174–179.
[46] J. Virkutyte, V. Jegatheesan, R.S. Varma, Visible light activated TiO_2/microcrystalline cellulose nanocatalyst to destroy organic contaminants in water, Bioresour. Technol., 113 (2012) 288–293.
[47] V. Gupta, D. Pathania, P. Singh, A. Kumar, B. Rathore, Adsorptional removal of methylene blue by guar gum–cerium (IV) tungstate hybrid cationic exchanger, Carbohydr. Polym., 101 (2014) 684–691.
[48] A. Einbu, Characterisation of Chitin and a Study of its Acid-Catalysed Hydrolysis, PhD Dissertation, Norwegian University of Science and Technology, Trondheim, 2007.
[49] E. Guibal, A. Larkin, T. Vincent, J. Tobin, Platinum recovery on chitosan-based sorbents, Process Metall., 9 (1999) 265–275.
[50] M.M. Ba-Abbad, A.A.H. Kadhum, A.B. Mohamad, M.S. Takriff, K. Sopian, The effect of process parameters on the size of ZnO nanoparticles synthesized via the sol–gel technique, J. Alloys Compd., 550 (2013) 63–70.
[51] M.M. Ba-Abbad, A.A.H. Kadhum, A.B. Mohamad, M.S. Takriff, K. Sopian, Visible light photocatalytic activity of Fe^{3+}-doped ZnO nanoparticle prepared via sol–gel technique, Chemosphere, 91 (2013) 1604–1611.
[52] M.-T. Yen, J.-L. Mau, Selected physical properties of chitin prepared from shiitake stipes, LWT Food Sci. Technol., 40 (2007) 558–563.
[53] R. Zhang, L.L. Kerr, A simple method for systematically controlling ZnO crystal size and growth orientation, J. Solid State Chem., 180 (2007) 988–994.
[54] Z. Ambrus, N. Balázs, T. Alapi, G. Wittmann, P. Sipos, A. Dombi, K. Mogyorósi, Synthesis, structure and photocatalytic properties of Fe(III)-doped TiO_2 prepared from $TiCl_3$, Appl. Catal., B, 81 (2008) 27–37.
[55] H.M. Gad, A.A. El-Sayed, Activated carbon from agricultural by-products for the removal of Rhodamine-B from aqueous solution, J. Hazard. Mater., 168 (2009) 1070–1081.
[56] A.V. Deshpande, U. Kumar, Effect of method of preparation on photophysical properties of Rh-B impregnated sol–gel hosts, J. Non-Cryst. Solids, 306 (2002) 149–159.
[57] M.R.R. Kooh, M.K. Dahri, L.B. Lim, The removal of rhodamine B dye from aqueous solution using *Casuarina equisetifolia* needles as adsorbent, Cogent Environ. Sci., 2 (2016) 1140553.
[58] V. Poots, G. McKay, J. Healy, The removal of acid dye from effluent using natural adsorbents—I peat, Water Res., 10 (1976) 1061–1066.
[59] S. Boutemedjet, O. Hamdaoui, Sorption of malachite green by eucalyptus bark as a non-conventional low-cost biosorbent, Desal. Wat. Treat., 8 (2009) 201–210.
[60] J. Huang, Y. Liu, Q. Jin, X. Wang, J. Yang, Adsorption studies of a water soluble dye, Reactive Red MF-3B, using sonication-surfactant-modified attapulgite clay, J. Hazard. Mater., 143 (2007) 541–548.
[61] M.J. Iqbal, M.N. Ashiq, Adsorption of dyes from aqueous solutions on activated charcoal, J. Hazard. Mater., 139 (2007) 57–66.
[62] D. Ghosh, K.G. Bhattacharyya, Adsorption of methylene blue on kaolinite, Appl. Clay Sci., 20 (2002) 295–300.
[63] A. Özcan, E.M. Öncü, A.S. Özcan, Kinetics, isotherm and thermodynamic studies of adsorption of Acid Blue 193 from aqueous solutions onto natural sepiolite, Colloids Surf., A, 277 (2006) 90–97.
[64] J. Eastoe, J. Dalton, Dynamic surface tension and adsorption mechanisms of surfactants at the air–water interface, Adv. Colloid Interface Sci., 85 (2000) 103–144.
[65] J.-W. Lee, T.-O. Kwon, I.-S. Moon, Adsorption of monosaccharides, disaccharides, and maltooligosaccharides on activated carbon for separation of maltopentaose, Carbon, 42 (2004) 371–380.
[66] Z. Al-Qodah, Adsorption of dyes using shale oil ash, Water Res., 34 (2000) 4295–4303.
[67] I. Langmuir, The constitution and fundamental properties of solids and liquids. Part I. Solids, J. Am. Chem. Soc., 38 (1916) 2221–2295.
[68] H. Freundlich, Over the adsorption in solution, J. Phys. Chem., 57 (1906) 1100–1107.
[69] V. Gupta, B. Gupta, A. Rastogi, S. Agarwal, A. Nayak, A comparative investigation on adsorption performances of mesoporous activated carbon prepared from waste rubber tire and activated carbon for a hazardous azo dye—Acid Blue 113, J. Hazard. Mater., 186 (2011) 891–901.
[70] I. Tan, A.L. Ahmad, B. Hameed, Adsorption of basic dye on high-surface-area activated carbon prepared from coconut husk: equilibrium, kinetic and thermodynamic studies, J. Hazard. Mater., 154 (2008) 337–346.
[71] V.S. Mane, I.D. Mall, V.C. Srivastava, Kinetic and equilibrium isotherm studies for the adsorptive removal of Brilliant Green dye from aqueous solution by rice husk ash, J. Environ. Manage., 84 (2007) 390–400.
[72] Theivarasu, S. Mylsamy, Equilibrium and kinetic adsorption studies of Rhodamine-B from aqueous solutions using cocoa (*Theobroma cacao*) shell as a new adsorbent, Int. J. Eng. Sci. Technol., 2 (2010) 6284–6292.
[73] G. Vijayakumar, R. Tamilarasan, M. Dharmendirakumar, Adsorption, kinetic, equilibrium and thermodynamic studies on the removal of basic dye Rhodamine-B from aqueous solution by the use of natural adsorbent perlite, J. Mater. Environ. Sci., 3 (2012) 157–170.
[74] F. Motahari, M.R. Mozdianfard, M. Salavati-Niasari, Synthesis and adsorption studies of NiO nanoparticles in the presence of H_2acacen ligand, for removing Rhodamine B in wastewater treatment, Process. Saf. Environ. Prot., 93 (2015) 282–292.
[75] J. Saini, V. Garg, R. Gupta, N. Kataria, Removal of Orange G and Rhodamine B dyes from aqueous system using hydrothermally synthesized zinc oxide loaded activated carbon (ZnO-AC), J. Environ. Chem. Eng., 5 (2017) 884–892.
[76] H. Chen, J. Zhao, Adsorption study for removal of Congo red anionic dye using organo-attapulgite, Adsorption, 15 (2009) 381–389.
[77] S. Lagergren, Zur theorie der sogenannten adsorption gelöster stoffe, K. Sven. Vetensk.akad. Handl., 24 (1898) 1–39.
[78] Y. Ho, G. McKay, The sorption of lead(II) ions on peat, Water Res., 33 (1999) 578–584.
[79] Y.-S. Ho, G. McKay, Sorption of dye from aqueous solution by peat, Chem. Eng. J., 70 (1998) 115–124.
[80] Y.-S. Ho, G. McKay, The kinetics of sorption of divalent metal ions onto sphagnum moss peat, Water Res., 34 (2000) 735–742.
[81] Y. Haldorai, J.-J. Shim, An efficient removal of methyl orange dye from aqueous solution by adsorption onto chitosan/MgO composite: a novel reusable adsorbent, Appl. Surf. Sci., 292 (2014) 447–453.